Time dependent microstructure of bitumen and its fractions by modulated differential scanning calorimetry

Masson, J-F.; Polomark, G. M.; Collins, P.

Publisher's version / Version de l'éditeur:
https://doi.org/10.1021/ef010233r
Energy & Fuels, 16, Mar-Apr 2, pp. 470-476, 2002-04-01

Time-dependent microstructure of bitumen and its fractions by modulated differential scanning calorimetry

Masson, J-F.; Polomark, G.M.; Collins, P.

NRCC-45137

A version of this paper is published in / Une version de ce document se trouve dans:
Energy & Fuels, v. 16, no. 2, Mar-Apr. 2002, pp. 470-476

Time-Dependent Microstructure of Bitumen and Its Fractions by Modulated Differential Scanning Calorimetry

J-F. Masson,* G. M. Polomark, and P. Collins

Institute for Research in Construction, National Research Council of Canada, Ottawa, Ontario, Canada, K1A 0R6

Received September 21, 2001. Revised Manuscript Received December 3, 2001

Bitumen fractions were analyzed by modulated differential scanning calorimetry (MDSC) before and after annealing at room temperature. MDSC allowed for separating glass transitions (T_g's) from order−disorder transitions. All fractions showed at least two T_g's and different states of order. Saturates were semicrystalline, aromatics were amorphous, resins, and asphaltenes were mesophasic. In bitumen, the fractions order in four stages upon cooling from the melt. In the first stage, all fractions order rapidly into a weakly organized phase. In the second stage, low molecular weight saturated segments crystallize. In the third stage, high molecular weight saturated segments crystallize. In the fourth stage, resins and asphaltenes order into a mesophase. The third and fourth stages are responsible for the room-temperature (steric) hardening of bitumen.

1. Introduction

Bitumen is an oligomeric material with a time-dependent microstructure[1] that affects viscoelastic properties.[2−4] After it is cooled from the melt, bitumen becomes harder over time; the hardening is defined by the storage temperature immediately after cooling. Physical hardening takes 1−2 days at −15 to −35 °C,[4] which is in the glass transition temperature (T_g) region for most bitumens. Steric hardening,[3] which occurs at room temperature, takes days to weeks. The two names for hardening imply that two mechanisms are responsible for hardening. On the basis of the simple Arrhenius relationship between rates and temperatures,[5] hardening would be expected to be faster at the higher temperature. Because this is not the case, at least two molecular mechanisms must govern the development of bitumen microstructure and, consequently, its hardening.

Physical hardening has been related to the loss of free volume at T_g,[6,7] and to the crystallization of the saturates.[7,8] Steric hardening has been attributed to the association of the asphaltenes,[3] which would explain the increased steric hardening upon oxidation.[9] However, maltenes (deasphaltenated bitumen) have also shown a time-dependent behavior.[10] Consequently, the exact molecular mechanism for steric hardening remains uncertain.

We have recently shown that modulated differential scanning calorimetry (MDSC) can be used to investigate the time-dependent behavior of bitumen.[1] When bitumen was cooled from the melt and annealed at 22 °C, its microstructure developed slowly and three stages were identified.

In this paper, MDSC is used to investigate the thermal behavior of bitumen fractions, to reveal the time dependency of their structure and provide a molecular basis for the steric hardening of bitumen. MDSC provides greater sensitivity than conventional DSC as it allows for differentiating between reversing and nonreversing thermal behaviors in bitumen (Figure 1). Reversing events include those that can be brought to equilibrium during the period of a modulated temperature signal used in the MDSC experiment.[11−14] Most important in this respect are the atomic motions

* Corresponding author. Tel: 1-613- 993-2144. Fax:1-613-952-8102. E-mail: jean-francois.masson@nrc.ca.

(1) Masson, J.-F.; Polomark, G. *Thermochim. Acta* **2001**, *374*, 105−114.
(2) Traxler, R. N.; Schweyer, H. E. *Proc. Am. Soc. Test. Mater.* **1936**, *36*, 544−550.
(3) Brown, A. B.; Sparks, J. W.; Smith, F. M. *Proc. Assoc. Asphalt Paving Technol.* **1957**, *26*, 486−494.
(4) Lu, X.; Isacsson, U. *Const. Build. Mater.* **2000**, *14*, 79−88.
(5) McQuarrie, D. A.; Simon, J. D. *Physical Chemistry: A Molecular Approach*; University Science Books: Sausalito, CA, 1997; p 1163.
(6) Anderson, D. A.; Bahia, H. U. *Proc. Assoc. Asphalt Paving Technol.* **1993**, *62*, 93−129.
(7) Anderson, D. A.; Marasteanu, M. O. *Transp. Res. Rec.* **1999**, *1661*, 27−34.
(8) Claudy, P.; Létoffé, J. M.; Rondelez, F.; Germanaud, L.; King, G.; Planche, J. P. *Prepr. Pap.−Am. Chem. Soc., Div. Fuel Chem.* **1992**, *37* (3−4), 1408−1426.
(9) Petersen, J. C. *Transp. Res. Rec.* **1984**, *999*, 13−30.
(10) Branthaver, J. F.; Petersen, J. C.; Robertson, R. E.; Duvall, J. J.; Kim, S. S.; Harnsberger, P. M.; Mill, T.; Ensley, F. A.; Barbour, F. A.; Schabron, J. F. *Binder Characterization and Evaluation*; Strategic Highway Research Program, National Research Council: Washington, DC, 1994; Vol. 2.
(11) Jones, K. J.; Kinshott, I.; Reading, M.; Lacey, A. A.; Nikopoulos, C.; Pollock, H. M. *Themochim. Acta* **1997**, *304/305*, 187−199.
(12) Lacey, A. A.; Nikopoulos, C.; Reading, M. J. *Therm. Anal.* **1997**, *50*, 279−333.
(13) Reading, M. *Trends Polym. Sci.* **1993**, *1*, 248−253.
(14) Gill, P. S.; Sauerbrunn, S. R.; Reading, M. *J. Therm. Anal.* **1993**, *40*, 931−939.

10.1021/ef010233r CCC: $22.00
Published on Web 02/05/2002

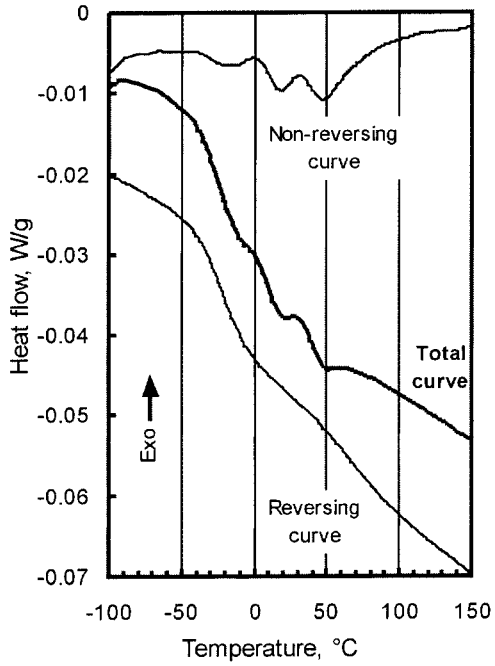

Figure 1. Total heat flow curve for bitumen. The curve separates into reversing and nonreversing components.

Table 1. Weight Percent Composition of Flash Chromatography Fractions as Measured by TLC-FID

	saturates	aromatics	resins A	resins B
heptane fraction	100	0	0	0
toluene fraction	0	51	45	4
THF fraction	0	0	93	7
asphaltenes from heptane	0	0	34	66

responsible for the heat capacity, C_p.[15] As a result, C_p is the major contributor to the reversing curve. Effects that cannot be modulated and brought to equilibrium are excluded from the reversing curve and show as nonreversing, e.g., oxidation, evaporation, decomposition, relaxation.[13] Melting and crystallization can include both reversing and nonreversing contributions.[13,16]

In this paper, it is shown that MDSC can be used to probe the time-dependent microstructure of the various fractions in bitumen, namely, the saturates, aromatics, resins, and asphaltenes. Moreover, the study reveals that each fraction shows at least two T_g's, and that the fractions contribute to a four-stage development of the microstructure in the original bitumen, instead of the three stages as originally indicated.[1] Two stages are related to the steric hardening of bitumen.

2. Experimental Section

Bitumen fractions rich in saturates, aromatics, resins, or asphaltenes were obtained by flash chromatography (FC).[17] The composition of the fractions as obtained by TLC-FID[18] is shown in Table 1. After a slow evaporation of the FC solvent at 85 °C, samples were placed in DSC pans and dried for 1 h at 150 °C under a flow of nitrogen. The pans were then sealed and the samples annealed for various times, the longest time being that when steady-state was achieved. This was verified by running samples periodically until no change was observed in the MDSC signal. Annealing as defined here is the storage at 22 ± 1 °C (room temperature).

MDSC heating and cooling curves were obtained at a rate of 3 °C/min with a modulation period of 60 s and an amplitude ±0.47 °C. All samples were subjected to the following thermal programs: (i) First heating: −100 to 150 °C (after rapid cooling from the annealing temperature). Rapid cooling is an exponential cooling rate fastest at the beginning of cooling. About 15 min is required for cooling, so that the average cooling rate is about 15 °C/min. The first heating provides results for the annealed samples. (ii) Second heating: −100 to 150 °C (after rapid cooling from the 150 °C). This step provides results for unannealed samples. (iii) Cooling from 150 to −100 °C.

The reversing heat flow was converted to heat capacity, C_p, by dividing the heat flow by the underlying heating rate. At T_g, the change in heat capacity was defined by its derivative as $\Delta C_p = \int (dC_p/dT)\, dT$. Details pertaining to the analysis are found elsewhere.[1]

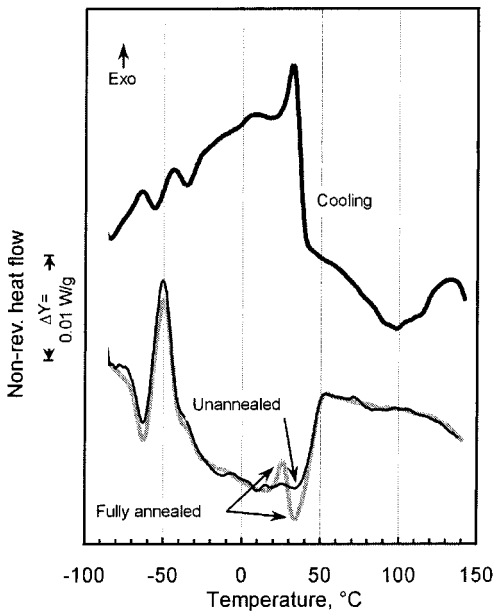

Figure 2. Nonreversible heat flow curves for the saturates showing the time dependence of the exotherm−endotherm pair at 20−50 °C indicating some steric hardning. The third curve shows ordering during cooling.

3. Results

3.1. Saturates. The nonreversing heat flow curves obtained from the heating and cooling experiments are shown in Figure 2. The simplest curve, obtained from cooling, shows multiple exotherms between 40 and −85 °C. Upon heating there is a broad endothermic background that corresponds to the broad exotherm obtained from cooling. As with the original bitumen,[1] a sharp low-temperature exotherm overlaps with the background. In the saturates, this exotherm is centered at −50 °C.

Annealing has an effect on the profile of the nonreversing heating curve between 20 and 50 °C. The annealed sample (first heating) shows a small exotherm at 27 °C, immediately followed by an endotherm of similar size centered at 35 °C. In the unannealed sample (second heating), these features are absent. However,

(15) Wunderlich, B. *Thermochim. Acta* **1999**, *340/341*, 37−52.
(16) Wunderlich, B.; Okazaki, I.; Ishikiriyama, K.; Boller, A. *Thermochim. Acta* **1998**, *324*, 77−85.
(17) Raki, L.; Masson, J-F.; Collins, P. *Energy Fuels* **2000**, *14*, 160−163.
(18) Masson, J-F.; Price, T.; Collins, P. *Energy Fuels* **2001**, *15* (4), *955−960*.

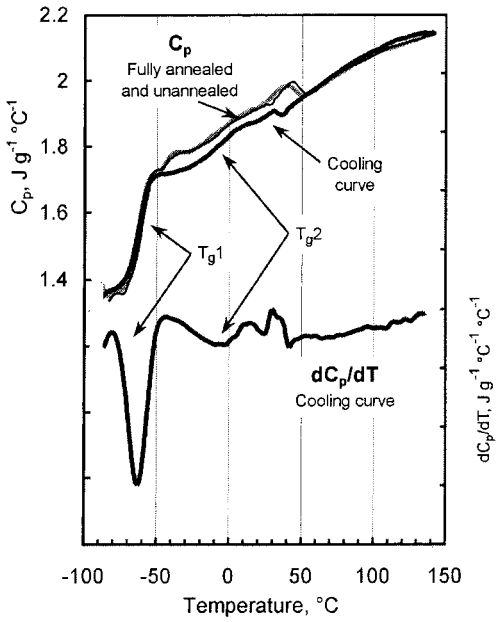

Figure 3. C_p curves for the saturates. The dC_p/dT curve helps to highlight the small T_g at −10 °C. The derivative signal between 10 and 50 °C is not a T_g, but arises from reversible melting. See text for details.

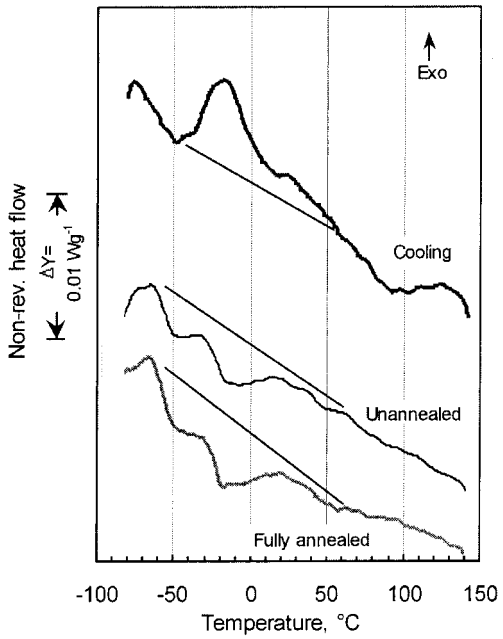

Figure 4. Nonreversing heat flow curves for the aromatics obtained upon heating (bottom). Time-independent behavior is shown by the similarity of the curves for annealed and unannealed samples. The upper curve shows an exotherm (ordering) during cooling. The baseline between about −50 and 50 °C helps visualize the exotherms and endotherms.

the endotherm−exotherm pair slowly reappears over 24 h, after which it is at steady state.

The heat capacity (C_p) curves obtained from the saturates are shown in Figure 3. The cooling curve is again the simplest. It reveals a strong glass transition (T_g) at −60 °C, a weak T_g at −10 °C, and a small fluctuation of the heat capacity between 25 and 40 °C. The heating curves show the same features, but the weaker T_g is more difficult to see because of fluctuations in C_p at −37 and 42 °C, and because of thermal hysteresis between −50 and 50 °C. The derivative, dC_p/dT, helps identify the T_g region and center the transition.

3.2. Aromatics. Upon cooling from 150 °C, the nonreversing heat flow from the aromatics shows a wide exotherm with a maximum at −15 °C (Figure 4). Upon heating there is a correspondingly broad endotherm and no exotherm rise above a baseline drawn from −60 to 60 °C.

The C_p curves are shown in Figure 5. There is an overlap of the heating and cooling curves and no thermal hysteresis. These curves show at least two T_g's, a strong one centered at −15 °C and a weak one at 65 °C, as confirmed with the derivative curve. There might also be a very weak T_g around −50 °C, which would be responsible for the slight asymmetry at the base of the derivative peak at −15 °C.

3.3. Resins. Typical nonreversing heat-flow curves for the resins are shown in Figure 6. The curve for the annealed sample shows a relatively large endotherm between −10 and 60 °C, but the curve for the unannealed sample only shows a small one. The cooling run shows an exotherm similar in size to the endotherm for the unannealed sample. When the resins are annealed at 22 °C, the endotherm returns to its full size in ~3 days (Figure 7).

The C_p curves for the resins are shown in Figure 8. Heating and cooling curves overlap and no thermal hysteresis is observed. In contrast to the main low-

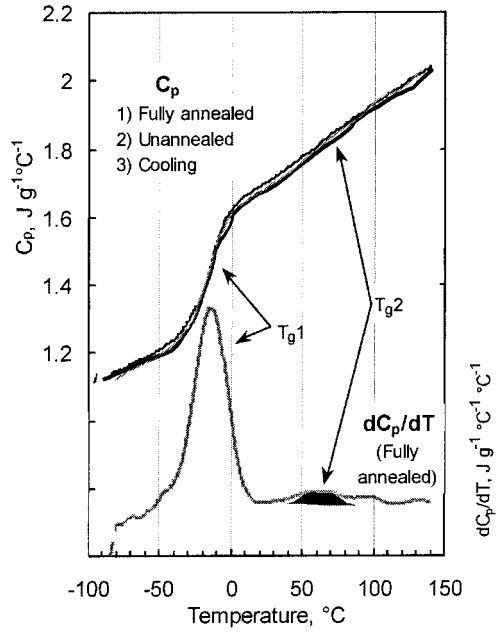

Figure 5. C_p curves for the aromatics after a first heating (annealed), second heating (unannealed), and cooling runs show no hysteresis, hence they overlap. The dC_p/dT curve reveals a second weak T_g at 70 °C, as shown by the black shade, and possibly a very weak T_g around −50 °C. See text for details.

temperature T_g of the aromatics, which is sharp, the resins show a broad low-temperature T_g. The dC_p/dT curve reveals the presence of two, possibly three, overlapping T_g's, as indicated by the dotted lines at the bottom of Figure 8. The larger T_g region, centered at 20 °C, overlaps with a small T_g at 70 °C and possibly another at −60 °C.

3.4. Asphaltenes. The nonreversing heat flow curves for fully annealed asphaltenes show an endotherm

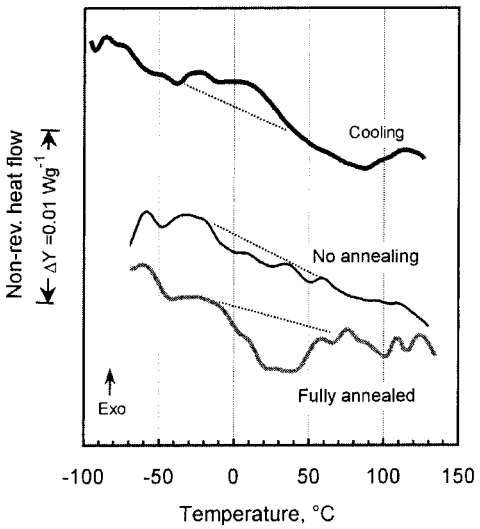

Figure 6. Nonreversing heat flow curves for annealed and unannealed resins are different as seen from the increased area under a baseline drawn from −20 to 60 °C (bottom). The upper curve shows the ordering of resins upon cooling from the melt.

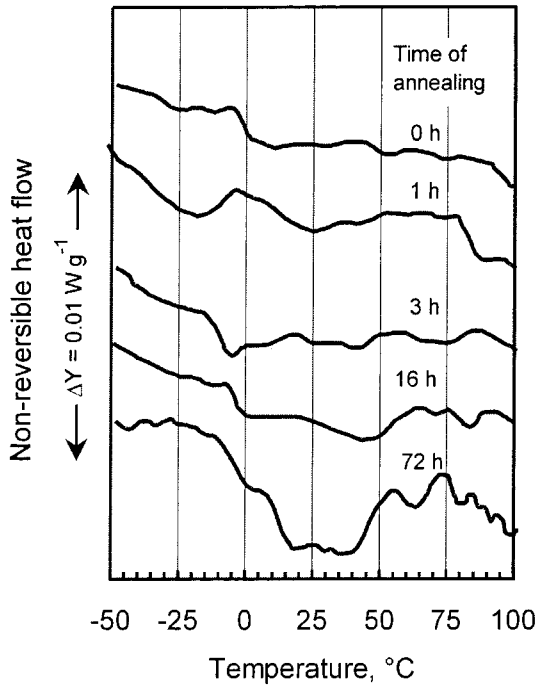

Figure 7. Time-dependent nonreversing heat flow curves for resins.

centered around 50 °C (Figure 9). The curve for the unannealed sample shows a small, broad endotherm similar in size to the exotherm of the cooling curve. When the asphaltenes are annealed at 22 °C, the endotherm increases to attain steady-state in ~14 days (Figure 10).

The C_p curves for the asphaltenes are shown in Figure 11. There is an overlap of the heating and cooling curves and no thermal hysteresis. The C_p curves have an extended S shape, which reveal an extraordinarily broad T_g region that extends over 200 °C. Two poorly resolved T_g's can be identified in the derivative curve. The dotted lines in Figure 11 show the deconvoluted T_g's. The first transition is centered at 0 °C and the other at 70 °C, with the latter being prevalent.

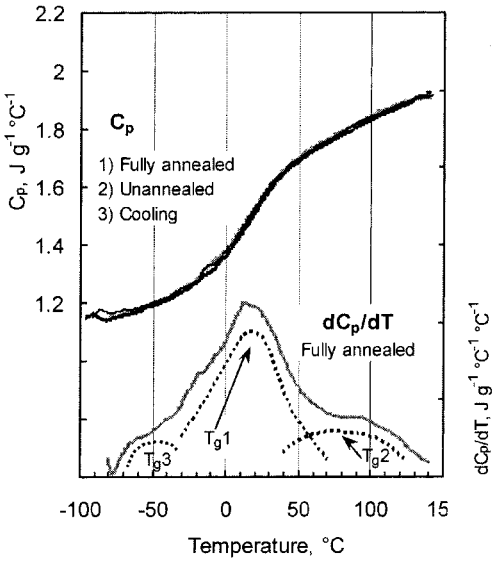

Figure 8. C_p curves for the resins show no hysteresis. The dC_p/dT curve reveals the existence of overlapping T_g's, as shown by the dotted lines.

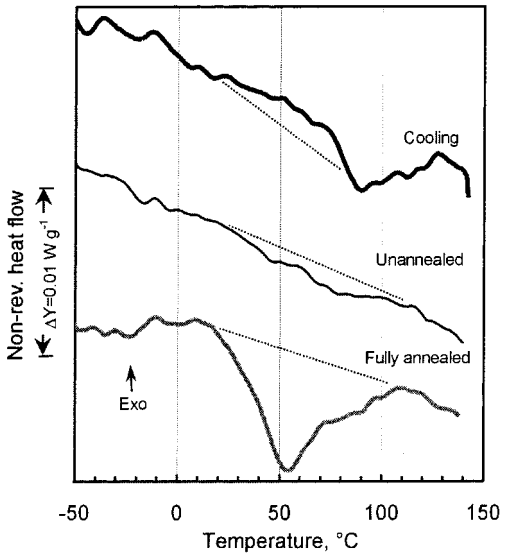

Figure 9. Nonreversing heat flow curves for annealed and unannealed asphaltenes are different as seen from the baseline (bottom). The exotherm of the upper curve shows the very slight ordering of asphaltenes upon cooling from the melt.

4. Discussion

4.1. Saturates. Saturates are semicrystalline.[8] The endotherms and exotherms shown by the saturates on the nonreversing curves arise from melting and crystallization (Figure 2). Upon cooling from 150 °C, the saturates crystallize because of nucleation, which typically begins at a supercooling of 30 to 100 °C.[19] The numerous peaks and the breadth of the exotherm obtained during cooling indicate that a myriad of crystalline structures develop upon cooling. The low temperatures of these peaks suggest that crystal density is low, in accordance with that for low-density polyolefins.[20] The low crystal density, which most likely

(19) Wunderlich, B. *Macromolecular Physics*; Academic Press: New York, 1976.

(20) Mathot, V. B. F. In *New Advances in Polyolefins*; Chung, T. C., Ed.; Plenum Press: New York, 1993; Vol. 2, pp 1−30.

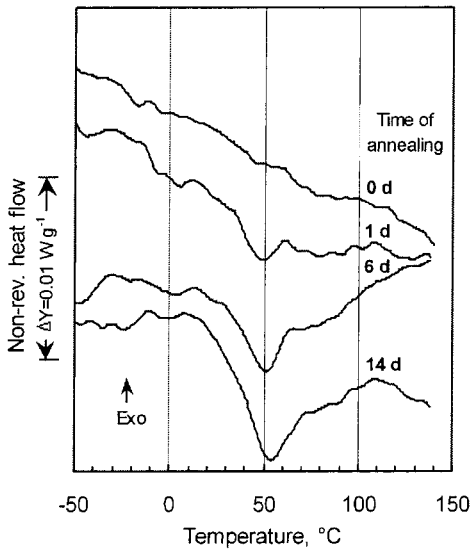

Figure 10. Nonreversing heat flow curves for asphaltenes annealed for 0 to 14 days.

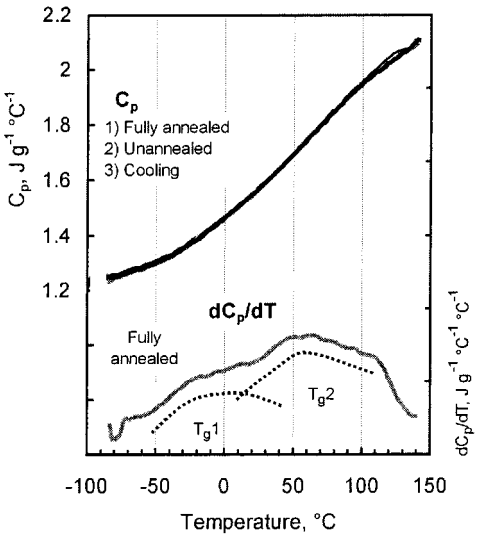

Figure 11. C_p curves for the asphaltenes show no hysteresis. The dC_p/dT curve shows the existence of two overlapping T_g's, as shown by the dotted lines.

arises from the polydispersity[21] and branching of the saturates,[22] also suggests that crystals are small and imperfect. This is confirmed by the existence of a cold crystallization exotherm at −50 °C on the heating curves.

Crystals formed upon cooling will melt during heating to provide the endothermic background. Within this background, exotherms mark the cold crystallization of some saturates. In this process, the small and imperfect crystals that formed upon cooling melt and recrystallize to larger crystals with higher melting points.[19] Thus, the intense cold crystallization peak at −50 °C first detracts and then contributes to the endothermic background. In the same background, the small cold crystallization peak at 27 °C gives rise to the small melting peak at 35 °C.

The heating curve for the unannealed saturates shows cold crystallization at −50 °C but not at 27 °C. It takes 1 day of annealing for the cold crystallization peak at 27 °C to reform. This indicates that cold crystallization at −50 and 27 °C arise from the melting and recrystallization of crystals built from segments of different sizes and with different diffusion rates. In polymers, an increase in molecular weight reduces the rate of diffusion and crystallization.[19] Hence, it is likely that with saturates small imperfect crystals with short saturated segments give rise to the cold crystallization at −50 °C, and those with longer, heavier and slower diffusing segments give rise to the cold crystallization at 27 °C. This transition would arise upon heating, but only after heavy segments have had sufficient time to properly group. These segments could be monosubstituted cycloaliphatics (naphthenes), which because of their larger molecular volumes would diffuse more slowly than aliphatic segments.

Crystallization and melting can contribute to C_p (Figure 3), although they are generally considered irreversible processes. They do so because imperfect crystals have a small region of metastability between crystallization and melting.[16] During the modulation cycle of the MDSC experiment, the crystals have time to perfect and melt. As a result, rapid melting and crystallization appear in the reversing curve. This reversible melting and recrystallization explains the thermal hysteresis in the heat capacity obtained by heating and cooling and the small rises in C_p, at −37 and 42 °C. Interestingly, the original bitumen showed no thermal hysteresis in its C_p curves,[1] which indicates that the saturates had a much lower state of ordering when blended with the other bitumen fractions. However, unpublished work shows that some bitumens exhibit thermal hysteresis.

The change in C_p for the saturates results not only from crystalline matter, but also from amorphous matter, which gives rise to two T_g's. The large T_g in the region from −75 to −50 °C is consistent with that obtained by regular DSC,[23] but here it is better resolved because of the absence of overlap with the cold crystallization peak at −50 °C. As a result, MDSC allows for a better assessment of ΔC_p at T_g than regular DSC. Moreover, in regular DSC, the small T_g at −10 °C is hidden in the endothermic background. This small T_g is only observed by MDSC because of the deconvolution of reversing and nonreversing events.

The positions of the two T_g's provide some indication of the structure responsible for the transitions. The T_g increases when the molecular structure becomes more rigid due to the increase in molecular weight, the presence of rings, or polar groups.[24] Consequently, the T_g at −60 °C arises from the most flexible segments of the saturates, whereas that at −10 °C arises from the most rigid segments. Given the presence of linear, branched, and cyclic structures in the saturates,[22] the higher T_g more likely results from the stiffest of those structures, i.e., the highly branched or cyclic structures. They would also provide for imperfect crystals from which cold crystallization could develop, in accordance

(21) Paramanu, S.; Pruden, B. B.; Rahimi, P. *Ind. Eng. Chem. Res.* **1999**, *38*, 3121−3130.
(22) Speight, J. G. *Chemistry and Technology of Petroleum*, 3rd ed.; Marcel Dekker: New York, 1999.
(23) Claudy, P.; Létoffé, J.-M.; King, G. N.; Brûlé, B.; Planche J.-P. *Fuel Sci. Technol. Int.* **1991**, *9*, 71−92.
(24) Shen, M. C.; Eisenberg, A. *Rubber Chem. Technol.* **1970**, *43*, 95−155.

with the nonreversing curve at steady-state. Consequently, cold crystallization arises after T_g,[19] or as seen here, at the end of the T_g region. The same is observed with bitumen.[1] Hence, upon heating above the frozen state defined by the T_g region, diffusion of saturated segments is again permitted and nearest-neighbor crystallizable segments can crystallize. This explains why cold crystallization occurs at −50 °C in the saturates (T_g at −61 °C), and −10 °C in bitumen (T_g at −20 °C).[1]

The T_g's of the saturates, which arise from amorphous matter, are not affected by annealing. In contrast, annealing does affect the internal order of poorly crystalline domains that contain slow diffusing crystallizable segments. These segments align over ∼24 h and lead to cold crystallization at 27 °C. In other words, they lead to steric hardening of the saturates. As a result, saturates will also contribute to steric hardening of bitumen. However, the effect may be small due to the weakness of the transition within the saturates, and their dilution and lower relative crystallization within bitumen, as indicated by the absence of thermal hysteresis in the original mixture.[1]

4.2. Aromatics. The nonreversing heat flow curves for the aromatics show no conspicuous exotherm and the C_p curves show no hysteresis (Figures 4 and 5). Aromatics thus lack a crystalline phase, but they are not completely disordered. Low intensity exotherms and endotherms in the reversing and nonreversing curves indicate the existence of order−disorder transitions. The ordered phase is likely a mesophase (an ordered amorphous phase), in contrast to the crystalline (ordered) and amorphous (disordered) phases.

The aromatics have a large T_g flanked by one or two weaker transitions. The T_g at 70 °C is observed in the original bitumen (Figure 1) and in all fractions that contain aromatic structures. This T_g likely arises from an aromatic structure common to all fractions except the saturates. Given that the intensity of the transition increases in the order aromatics < resins < asphaltenes, it may arise from multi-ring structures, whose concentration increase in the same order.[22] In contrast, the presence of a very weak T_g around −50 °C is uncertain, but it would be consistent with the existence of saturated segments bonded to more rigid molecules that give rise to the T_g region centered at −15 °C.

The position of the thermal events in both the reversing and nonreversing curves were not affected by annealing. Hence aromatics did not contribute to steric hardening of bitumen. It is noteworthy, however, that aromatics fractionated from other bitumens have shown exotherms that rise above a baseline drawn from −60 to 100 °C.[25] It is likely that aromatics with long or stereoregular saturated segments can crystallize. Hence, like the saturates, they may contribute to steric hardening.

4.3. Resins. The nonreversing heat flow curves show no exotherm and the C_p curves for the resins show no hysteresis (Figures 6 and 8). The resins are thus mostly, if not completely, amorphous. The presence of two, possibly three, T_g's highlights the existence of distinct structural segments in resins, whereas the breadth of the main T_g, 85 °C, is consistent with that of a multi-component mixture. Like the aromatics, the resins show a T_g centered at 70 °C. The relative intensity of that transition indicates that the structures from which it arises are in greater concentration in the resins than in the aromatics. The T_g around −60 °C is somewhat uncertain, but it is close to that for saturates. This T_g would be consistent with the presence of saturated segments in resins, as postulated by Speight,[26] and the strong methylene and methyl absorbances in infrared spectra of resins.[27]

The T_g's of the resins are not affected by annealing, as the C_p curves remain unchanged over time. In contrast, the nonreversing curve is time-dependent (Figure 7). The growth of an endotherm due to ordering of the resins indicates that they play a role in the steric hardening of bitumen. From the amorphous nature of the resins, the relatively high aromaticity,[21] and the somewhat slow ordering process, it is likely that this fraction forms a mesophase whose order is high enough to provide an endotherm in the nonreversing curve, but not high enough to affect T_g.

4.4. Asphaltenes. Like the resins and the aromatics, the asphaltenes show no exotherm in the nonreversing heat flow curves obtained upon heating, and no thermal hysteresis in the C_p curve (Figures 9−11). They thus lack a crystalline phase, but like the resins they have an ordered amorphous phase. Indeed, a mesophase grows over ∼2 weeks, which is seen as an endotherm of increasing size at 50 °C (Figure 10). At steady-state, the size of the endotherm is larger than that of the resins. The asphaltenes thus contribute the most to the steric hardening of the original bitumen.

The amorphous domains in asphaltenes give rise to two extraordinarily broad and poorly resolved T_g's (Figure 11). The breadth of the transitions indicates that asphaltenes are polydisperse and heterogeneous. In other words, each T_g could be the overlap of several small T_g's. As T_g increases with the polarity, aromaticity, and molecular weight of the amorphous phase from which it originates,[24] the T_g at 0 °C may arise from polar aliphatic segments whereas that at 70 °C may arise from oligo-aromatic structures. The higher relative concentration of these structures in the asphaltenes may be responsible for the higher intensity of the T_g at 70 °C as compared with the other fractions. The T_g's for the asphaltenes is independent of time.

4.5. Bitumen. The thermal curves for bitumen are more than the sum of its fractions. Nonetheless, there are some similarities between the nonreversing curves that makes it possible to relate the features of the bitumen curve to individual fractions as shown in Figure 12. Four stages, instead of three as reported earlier,[1] were identified in the development of bitumen microstructure. A rapid first stage, which overlaps with the second one provides the endothermic background. As demonstrated earlier,[1] the background arises from the rapid ordering of saturated and aromatic segments upon cooling. As shown here, it arises from all fractions, but asphaltenes contribute the least. This ordering may be orchestrated by a collection of weak intermolecular interactions between alkylated and aromatic segments

(25) Masson, J-F.; Polomark, G. Unpublished results.

(26) Speight, J. G. *Chemistry and Technology of Petroleum*, 2nd ed.; Marcel Dekker: New York, 1981; p 441.

(27) Christy, A. A.; Dahl, B.; Kvalheim, O. M. *Fuel* **1989**, *68*, 430−435.

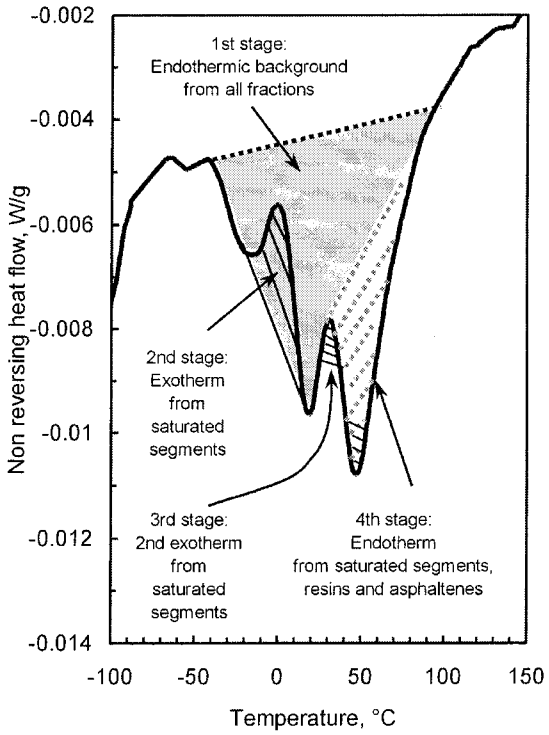

Figure 12. The nonreversing heat flow curve for the original bitumen, and the origin of the various stages of microstructure development. Stages 3 and 4 are responsible for steric hardening.

in an arrangement that facilitate the interactions of C−H bonds with π-electrons. The CH/π interaction is the weakest of the hydrogen bonds, but it is ubiquitous. As a result, it is thought to govern the conformation of many chemical systems,[28] and it may play an important role in bitumen microstructure. The second stage arises from the crystallization of low molecular weight saturated segments in saturates and other fractions, a process that takes about 3 h.[1] It is noteworthy that the original bitumen showed no thermal hysteresis in its C_p curves,[1] which indicates that the saturates had a much lower state of ordering when blended with the other fractions.

The third and fourth stages overlap (Figure 12). This is not immediately clear and it makes for a confusing curve and difficult analysis of bitumen that is only resolved by the analysis of its fractions. The third stage relates to a time-dependent crystallization of high molecular weight saturated segments. The process is similar to that of the second stage, but it is slower as seen with the fractions. The fourth stage, the development of an endotherm at 40−50 °C, is the slowest stage, which arises from resins and asphaltenes mesophases. Upon heating, there is an overlap of a melting peak from the saturated segments that crystallize in the third stage with the isotropization of resins and asphaltenes mesophases.

It is the time-dependent development of bitumen microstructure that causes the room-temperature steric hardening of bitumen. Stages 3 and 4 are thus responsible for steric hardening. Work on the bitumen fractions indicates that saturates contribute slightly to steric hardening, resins contribute more, and that asphaltenes contribute the most.

5. Conclusion

Bitumen fractions rich in saturates, aromatics, resins, or asphaltenes were analyzed by MDSC both before and after annealing at room temperature. MDSC allows for the separation of T_g's from order−disorder transitions. The C_p curves revealed at least two T_g's for each fraction, and the combined C_p and nonreversing heat flow curves allowed for an assessment of the state of order of each fraction.

The saturates showed thermal hysteresis between the heating and cooling C_p curves due to crystallinity. The nonreversing curve showed exothermic signals from two distinct crystalline phases. At low temperatures, a first phase develops immediately upon cooling from the melt. A second phase develops slowly over 1 day at room temperature. This second phase contributes to steric hardening. In contrast, the aromatics contained little crystalline material, if any, and showed no time dependence, and thus no steric hardening. However, aromatics that can crystallize may contribute to steric hardening. The resins and the asphaltenes were both affected by annealing, as time allowed for the formation of a phase of intermediate order between the amorphous and crystalline phases, i.e., a mesophase. Resins and asphaltenes achieved steady state in about 1 and 14 days, respectively. This indicated that both fractions contribute to steric hardening of bitumen.

A comparison of the nonreversing thermal curves for the original bitumen and its fractions allows for the identification of four stages in the development of bitumen microstructures. Steric hardening is the result of two mechanisms, i.e., the third and fourth stages. The third stage is the slow crystallization of high molecular weight saturated segments, e.g., cycloaliphatics, and the fourth stage is the slow formation of a mesophase due to resins and asphaltenes. The contribution of the asphaltenes to steric hardening is predominant, but that of the maltenes is not negligeable. They have a large influence on the kinetics aspect. For example, asphaltenes alone showed hardening during 14 days, but the original bitumen showed hardening during only 2−3 days.

There are three corollaries to this study. First, the increased concentration of resins and asphaltenes in oxidized bitumen explains the increased steric hardening of oxidized or blown bitumen over the unoxidized material. Second, the rheological testing of bitumen, which is most often started 1 h after cooling from the melt, would gain in reproducibility if started 24 h after cooling when much of the bitumen microstructure has redeveloped. Third, like its fractions, bitumen shows multiple T_g's. It is therefore likely that physical hardening, which occurs below T_g, is related to all the T_g's, and not only to the most intense, sub-zero T_g. This would explain the paradoxal physical hardening that seems to occur above T_g.

EF010233R

(28) Nishio, M.; Minoru, H.; Umezawa, Y. *The CH/π Interaction: Evidence, Nature and Consequences*; Wiley-VCH: New York, 1998.